Int. J. Heat Mass Transfer. Vol. 36, No. 12, pp. 2965–2976, 1993
Printed in Great Britain

0017–9310/93 $6.00+0.00

Heat transfer enhancement in a serpentine channel

B. SNYDER, K. T. LI and R. A. WIRTZ
Mechanical Engineering Department, University of Nevada–Reno, Reno, NV 89557, U.S.A.

(*Received* 9 *June* 1992 *and in final form* 12 *January* 1993)

Abstract—Forced-convection heat transfer rates and pressure drops were measured in the thermally fully developed region of a serpentine channel over Reynolds numbers ranging from 250 to 10000. The wall geometry was similar to # 17.8–3/8W of Kays and London [*Compact Heat Exchangers* (3rd Edn), p. 204. McGraw-Hill, New York (1984)], but carefully designed to minimize the extent of flow separation. The spatially-periodic wall impingement currents and high shear stresses combined to make a more uniform streamwise variation in local heat flux compared with corrugated surfaces. On an equal-*Re* basis, the heated surface of the serpentine channel outperformed the baseline parallel-plate channel by about a factor of 9 in air and 14 in water. Thus wavy-walled channels may prove effective for enhancing heat transfer in laminar and transitional flow regimes.

INTRODUCTION

CURRENT designs of plate-fin heat exchangers incorporate offset-strip fins, louvers, or flutes to interrupt the thermal boundary layer and thereby increase the overall heat transfer coefficient [1, 2]. Effective dispersion and mixing can also be promoted by deliberately inducing flow separation through the use of sharp-edged corrugations [3]; or by means of wavy-wall channels whose contours are made out-of-register [4]. High augmentation has also been produced by exciting destabilized Tollmein–Schlichting waves, either through the use of transverse grooves imbedded in the channel wall [5] or by cylinders placed spanwise to the flow [6]. Since leading edges and local flow separation cause large pressure drops, these devices all produce significant and unwanted increases in pumping power requirements.

By contrast, the present study utilizes the recursively-curved walls of a serpentine channel to induce spatially-periodic axial secondary flow. Because boundary-layer growth is repetitively interrupted by the reversal of wall curvature, boundary layers remain thin even in the 'fully-developed' regime where flow becomes phase-locked to the wall geometry. This design is therefore similar in concept to a ribbed-wall channel, except that flow separation is minimized by careful selection of the wall curvature. As a result, augmented heat transfer is achieved with only moderate increases in pumping power requirements, at least in the laminar and transitional flow regimes appropriate to current compact heat-exchanger technology.

In this paper we report some observations of flow visualization, and compare heat transfer/pressure drop measurements obtained for a serpentine test section with the performance of similar devices for which the flow patterns are also thought to be primarily two-dimensional. It will be shown that the present channel yields comparable performance and therefore provides an important addition to the repertoire of manufacturable compact-heat-exchanger designs.

EXPERIMENTAL DESIGN

Figure 1 shows an edge view of the serpentine channel segment, with numerical values of the geometric parameters listed in the accompanying caption. The channel design consists of 30 recursive arc circles with centerline radius of curvature R, peak-to-peak amplitude b, and periodicity length λ. The channel walls are of uniform width W and are separated by a uniform height H, resulting in a constant cross-sectional area normal to the flow direction.

Experiments were performed with water using a temperature-controlled recirculating water tunnel, and with air using an induced-draft wind tunnel. Water experiments used the facility shown in Fig. 2(a). A centrifugal pump delivered distilled water through a bank of rotameters and control valves to the left side of a partitioned reservoir which contained a cooling coil for temperature control. The right side of the tank was fed via a weir at the top of the partition and could supply up to a 1.2 m head to the test channel. The flow passed two honeycomb sections and entered a channel flow development section through a 'soda straw' flow straightener. This section had height $H = 10$ mm, width $W = 203$ mm, and length $L = 2440$ mm. The bottom and side walls of the section were aluminum, and the top surface was Plexiglas to permit visualization of the entering flow. Laser velocimetry measurements showed that the flow development length was sufficient to assure fully developed conditions at the test section inlet.

The open-loop wind tunnel shown in Fig. 2(b) included in sequence an entrance plenum, a flow development section ($L = 1220$ mm), the test section, and an exit plenum. Air was drawn through the system by a variable speed blower. Flow rate was monitored by a calibrated rotameter located downstream from the

NOMENCLATURE

b	peak-to-peak amplitude of wall waviness	Re	Reynolds number based on hydraulic diameter
D	hydraulic diameter	T_s	temperature of heated surface
f	Fanning friction factor	T_0	fluid inlet temperature; temperature of unheated surface
Gr	Grashof number, $g\beta L^3\Delta T/\nu^2$	ΔT	temperature difference, $T_s - T_0$
h	heat transfer coefficient	V	flow-average velocity
H	channel height	W	channel width
k	fluid thermal conductivity	x	entrance length.
K	entrance loss coefficient		
L	section length		
L_d	lengthscale for thermal development		
Nu	Nusselt number	Greek symbols	
Δp	pressure difference	β	$\Delta\rho/\rho$ buoyancy parameter
Pr	Prandtl number	λ	wall wavelength
q''	wall heat flux	ν	kinematic viscosity
R	centerline radius of curvature	ρ	fluid density.

exit plenum. An entrance nozzle with an 8:1 area ratio was located inside the entrance plenum. In combination with flow vanes inserted into the first 250 mm of the flow development section, this nozzle effectively eliminated disturbances in the entering flow, as verified using smoke to visualize the flow.

Flow visualizations were performed with water using a transparent full-scale model of the serpentine channel, constructed from vacuum formed acrylic. These studies used a pH-sensitive dye which, while ordinarily colorless, formed an intense magenta sheet when an electric pulse was passed through a thin wire electrode placed spanwise to the flow. A camera located above the channel recorded a plan-view of the evolving secondary flow. Heat transfer/pressure drop measurements were carried out using an identical channel geometry whose upper and lower contours were of aluminum, thinly coated with epoxy (0.08 mm) for corrosion resistance. The wavy section of the upper wall had a pattern of heaters bonded to its outer surface in order to maintain it at an elevated, uniform temperature, T_s. Its leading edge was thermally insulated from the adjoining flat channel section using a minimum contact area fiber gasket, so that flow along the upper channel wall was exposed to nearly a step change in wall temperature. The lower wavy wall had a cooling jacket attached to its outer (back) surface in order to maintain it at the entrance flow temperature, T_0. Copper–constantan thermocouples referenced to the inlet fluid temperature were imbedded along the midline of each wall, and at spanwise offsets, to check that the isothermal condition was maintained to within ± 0.3°C at all points along both surfaces.

Local heat transfer measurements were made along the centerline of the upper wall, thirteen waves downstream from the entrance. This segment of the wall was therefore replaced by an instrumented aluminum insert, fabricated as shown in Fig. 3. Six copper–constantan thermocouples were imbedded in grooves milled in the wavy surface, with lead wires run through holes at each end of the groove. The thermocouple junctions were peened flush with the wavy surface; the lead wires epoxied in place; and the surfaces filed smooth. Seven 5 mm by 50 mm silver–constantan heat flux gauges were then imbedded in a 0.5 mm thick polyimide coating which was molded to the wavy surface such that the resulting surface contour matched the rest of the wavy wall. During operation thermocouple measurements of surface temperatures in this coated segment were found to agree within 0.2°C of upstream temperatures, indicating that any effect of the polyimide layer was negligibly small. Edge effects also were kept negligible by centering the heat flux gauges on the midpoint of the channel span, 75 mm distant from the insulated sidewalls.

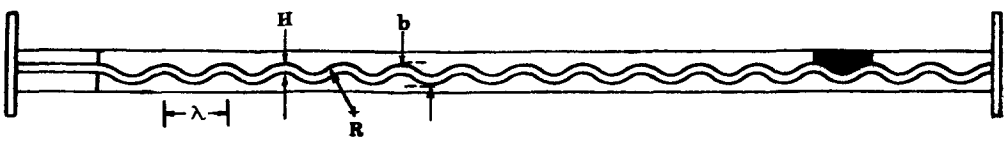

FIG. 1. Edge view of the wavy-wall channel, with channel spacing $H = 10.5$ mm, centerline radius of curvature $R = 30$ mm, wall wavelength $\lambda = 74.2$ mm, and peak-to-peak amplitude $b = 23.3$ mm. The channel aspect ratio $W/H \approx 19$. The fully-instrumented segment (shaded) is located 13 geometric waves downstream from the entrance at left.

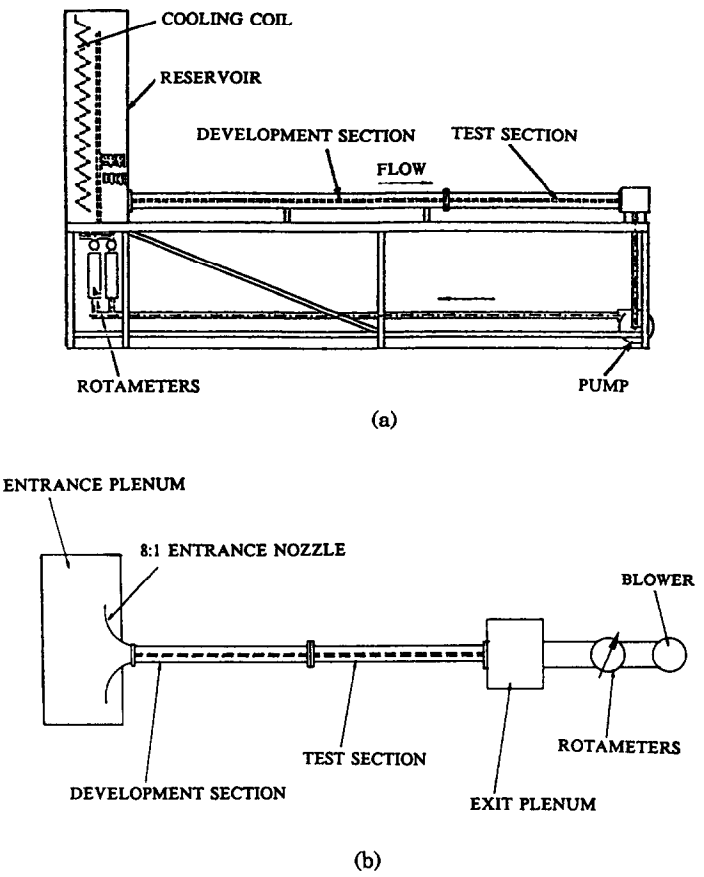

FIG. 2. (a) Closed loop test apparatus for water experiments. (b) Open loop test apparatus for air experiments.

Each heat flux gauge was calibrated in situ using three different conducting materials: water, glycerine and neoprene/styrene rubber. Since water or glycerine under zero-flow conditions produced marked qualitative effects of natural convection, a porous sponge was inserted into the lumen separating the two conducting walls to suppress any secondary flow. When saturated, this sponge weighed twenty times its dry weight, so that the effective thermal conductivity, k, must have closely approximated that of the pure liquid.† A third calibration utilized tightly-sandwiched sheets of rubber, which were bonded to the channel walls. Figure 4 shows that all three data sets yielded calibration slopes that agreed, on average, to within $\pm 5\%$. After accounting for minor variations in wall spacing, we attribute an uncertainty of $\pm 7\%$ to each individual calibration and an overall uncertainty of $\pm 3\%$ in the determination of section-averaged heat flux.

Due to funding constraints only one channel wall could be fully instrumented, which precluded any possibility of using a standard calorimetric balance to analyze heat transfer from symmetrically-heated walls. In principle the performance of the single heated surface could have been evaluated directly from knowledge of the local fluid temperature adjacent to each heat flux gauge. In practice such measurements would have been too imprecise to yield valid estimates of wall-fluid temperature differences. Instead, heat transfer from the instrumented segment of the heated surface was assessed using the heat balance shown in Fig. 5 (top panel). Provided that flow is thermally fully-developed (in a highly restrictive sense!) then heat convected from the upper wall is matched by heat lost to the cooled lower surface. Then the wall temperature difference $\Delta T = (T_s - T_0)$ could be used, instead of local mixed-mean temperature differences, to evaluate heat transfer coefficients.

To assess the extent to which flow became thermally fully-developed during actual operating conditions we measured local air temperatures midway between the top and bottom walls, by inserting thermocouples into the airstream through taps drilled at successive crests along the upper heated surface. These individual readings were than mapped to obtain a streamwise temperature profile extending throughout the entire

†If anything, this value of k underestimates the heat flux, and therefore provides a conservative estimate of performance.

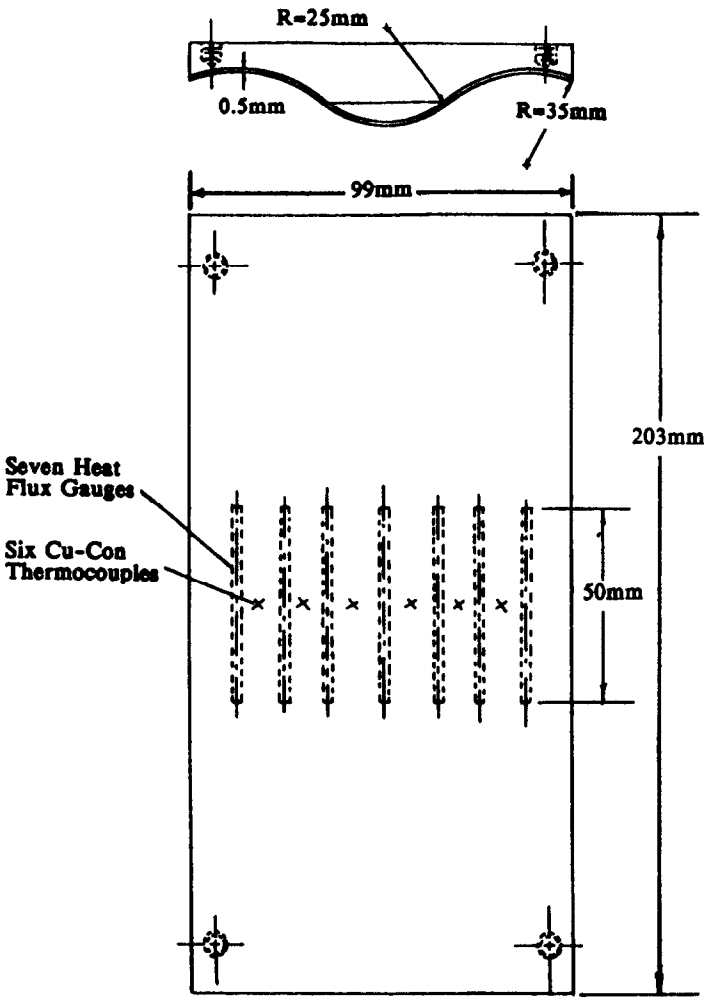

FIG. 3. Arrangement of heat flux gauges and thermocouples within the thirteenth wave segment. The surface of this segment was made of polyimide, 0.5 mm thick, to minimize heat flow between gauges.

test section, as shown in Fig. 5 (bottom panel). Each such trace was fitted to an exponential curve $(1-\exp[-(x-50)/L_d])$ to determine the length L_d which characterized thermal development. In laminar flow we found $L_d = 17.3\ Re^{0.305} \pm 5$ mm, with $L_d = 210 \pm 5$ mm nearly constant for $Re \geq 4000$. Thus for $Re = 250$, with $L_d = 90$ mm, the temperature of fluid entering the instrumented segment 980 mm downstream was within 0.1% of its asymptotic temperature. For $Re = 6000$, flow entering this segment was within 1.2% of its asymptotic temperature and rose only an additional 0.4% during passage through it.

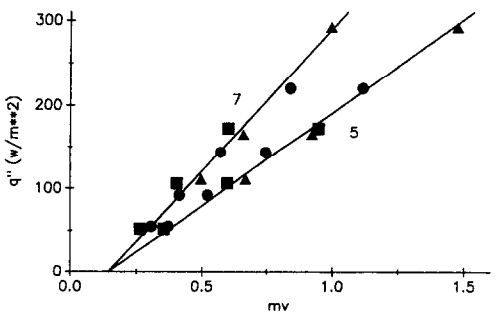

FIG. 4. Heat-flux calibrations using water (triangles), glycerine (circles) and rubber sheet (squares), for two individual gauges. For gauge 5 the slope is 223.2 ± 7.4 W m^{-2} mV^{-1} and for gauge 7, 349.2 ± 33.7 W m^{-2} mV^{-1}. The voltage offset was 0.14 mV for all seven gauges.

Fluid-wall temperature differences were too small to make meaningful measurements for water. Effects of Prandtl number were estimated by assuming that $L_d = 17.3\{7.9^{0.305}\}Re^{0.305}$, where the factor in braces accounts for the Pr ratio of water to air. Since Pr is typically less dominant than Re, this expression is likely to conservatively over-estimate the required entrance length for water. Thus flow entering the instrumented segment at $Re = 6000$ may have reached only 90% of fully-developed ΔT, rising a further 1.6% upon exit. At large Re, then, heat convected out from the instrumented segment may have falsely raised augmentation by perhaps 10–20%. The primary focus of this report, however, is with augmentation occurring

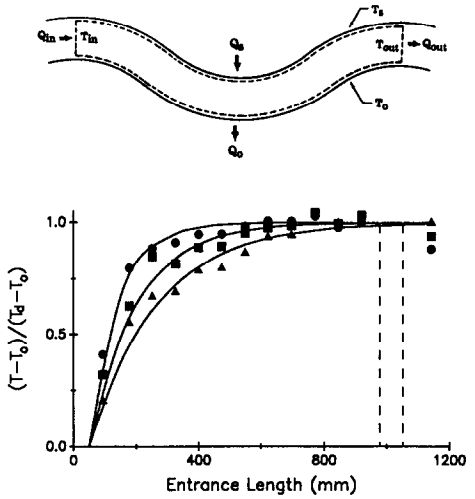

FIG. 5. Top: Heat balance used to assess heat transfer from instrumented segment of upper wall. In the thermally-developed region $Q_{in} = Q_{out}$, so that heat gained Q_s from heated upper surface equals heat lost Q_0 to cooled lower surface. Bottom: Streamwise centerline temperature profiles in air, for $Re = 250$ (circles), 1000 (squares) and 6000 (triangles). Each curve represents least-squares fit to data, using equation given in text. Dashed lines denote location of the instrumented segment.

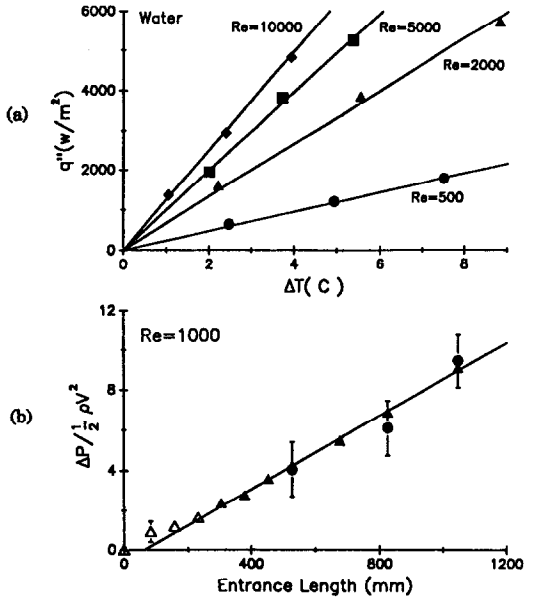

FIG. 6. (a) Dependence of area-averaged wall heat flux q'' on wall temperature difference $\Delta T = T_s - T_0$ for water. (b) Pressure drop vs downstream axial location in serpentine geometry at $Re = 1000$ for water (triangles) and air (circles). Open triangles represent measurements in the developing flow regime, and were excluded in computing slopes for friction factors (solid line).

at Re smaller than this, for which the reported data are likely to be indistinguishable from those taken under rigorously fully-developed conditions.

Heat transfer measurements were conducted over the Reynolds number range $250 \leqslant Re \leqslant 10\,000$, with Re based on the channel hydraulic diameter. Since the wall heat flux was non-uniform, the trapezoidal rule was used to spatially average q'', the heat flux per unit projected area, over the streamwise length of the instrumented segment for each given set of flow and surface heating rates. The wall temperature difference ΔT was varied; q″ was then plotted vs ΔT; and the slope of the resulting line was interpreted as the spatially-averaged heat transfer coefficient, h. In the case of the water data, q'' was closely linear with ΔT over the range $0 < \Delta T < 8°C$ and h could be obtained directly as in Fig. 6(a). When air was used q'' was still linear, but a correction was necessary to account for radiative heat transfer from the heated surface. Since the heat transfer data could be evaluated more directly in the case of water, the air data were useful largely in corroborating and supplementing these latter results.

Measurements of pressure drop were taken at specified flow rates using pressure ports located on the channel centerline at each wave crest along the upper channel wall. Data for water were obtained using a hook gauge with a sensitivity of ± 0.004 mm H_2O. Air data were measured by a differential pressure manometer which had an instrumental precision of ± 0.025 mm H_2O, but signal fluctuations limited the useful precision of the device to ± 0.1 mm H_2O. At high Re this noise contributed less than 1% uncertainty to the measured signal, but formed such a considerable portion of the total measurement at low Re that no useful data could be obtained for $Re < 500$.

The more precise results obtained for water made it clear that there was a small but not negligible effect of the entrance profile on overall pressure drop. For a typical case the frictional pressure gradient, as represented by the slope of the least-squares-fitted line in Fig. 6(b), first became fully-developed three wavelengths downstream from the entrance section. These data were correlated to the expression

$$\Delta p/\tfrac{1}{2}\rho V^2 = 4f\frac{x}{D} + K$$

where f is the Fanning friction factor and x is the distance between the inlet and downstream taps. The entrance loss factor $K = -0.48 \pm 0.22$ SD indicates a net decrease in kinetic energy, consistent with the transformation from parabolic inlet flow to a blunter downstream profile. Both air and water gave consistent results within experimental precision but only the water data permitted a resolution of the entrance loss K; thereby yielding higher, more conservative estimates of friction factors. These values, therefore, were used to construct the performance curves given elsewhere in this report.

FLOW VISUALIZATION AND ANEMOMETRY

A typical flow pattern obtained by embedding an electrode spanwise to the stream in the wall boundary layer is shown in Fig. 7(a). This visualization, taken

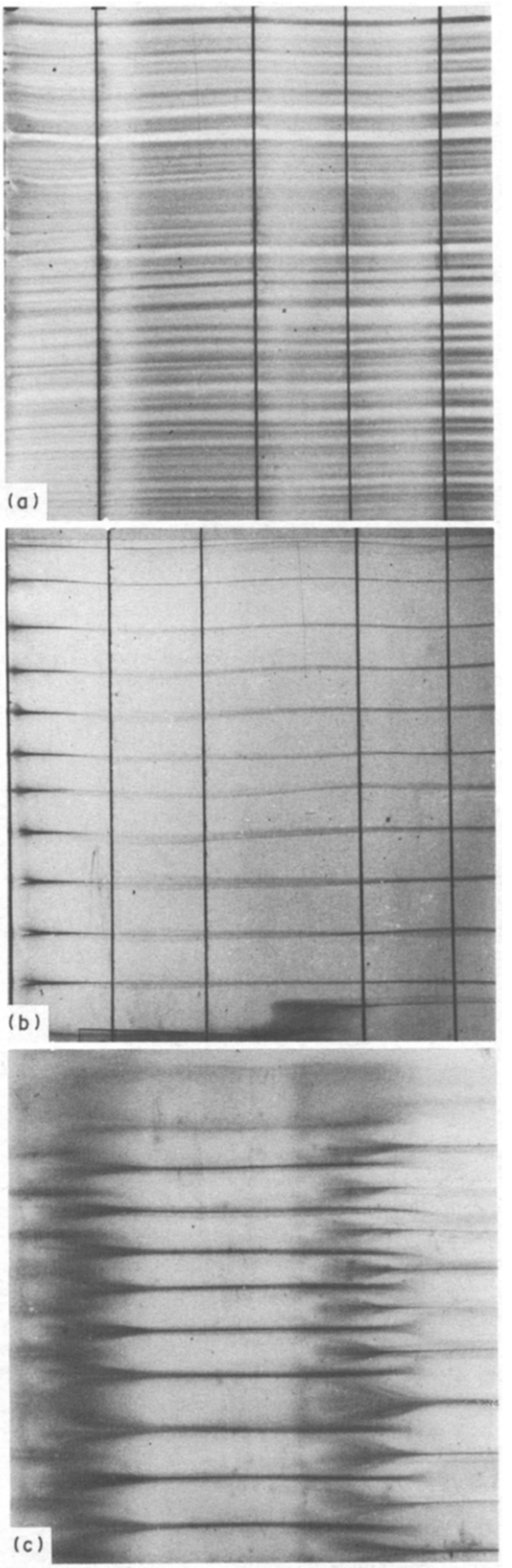

at $Re \sim 100$, represents the end-state of an evolving pattern, originating from an initially uniform dye front which gradually coalesced to form spanwise periodic braiding patterns characteristic of counter-rotating Goertler vortex pairs. Similar patterns have been reported by Goldstein and Sparrow [7] for a corrugated-wall channel. At somewhat higher $Re \sim 250$ this characteristically narrow Goertler array (2.6 mm) was supplanted by the much broader flow structure seen in Fig. 7(b). Its spacing, 10.6 mm, corresponds approximately to the channel separation H. Approximately two geometric wavelengths downstream of the initial visualization, this latter array was observed to undergo the complicated exchange process shown in Fig. 7(c). Adjacent braids first coalesced; then bifurcated to return 'in-register' with the upstream spacing pattern. The recursive wall geometry is probably accountable for this effect: a recent analytical study [8] suggests that periodic reversals of wall curvature may transform counter-rotating Goertler arrays into different cellular patterns. Moreover, the absence of such coalescing patterns in the upstream segment of dye trace implies an advective lag: thus an upwelling process may be required to form the ultimate cellular structure. Such secondary flows were observed to persist up to $Re \sim 450$, at which point either strong wall shear or local disturbances obliterated the patterns as soon as they formed.

Braiding was also observed to form immediately on the onset of wall curvature at the leading edge of the test section, but not upstream of this point. Swearington and Blackwelder [9] have reported that the spanwise spacing of primary Goertler vortices in a singly-curved channel is insensitive to Re number. Likewise, we found that these initial Goertler arrays had practically the same separation distance of 2.6 mm as those shown in Fig. 7(a), but persisted over a much more extended range $50 \leqslant Re \leqslant 1000$.

The visualization studies were supplemented by hot-wire measurements of the axial velocity profile in flowing air, taken at several representative stations within the 'fully-developed' region of the channel, 12–14 wavelengths downstream from the inlet. When assembled in sequence, these profiles exhibit the spatially-periodic pattern of secondary motion shown in Fig. 8 (top). Within this 'fully-developed' region flow becomes 'phase-locked' to the geometry, so that during each flow cycle the axial skew grows and declines in regular fashion within the geometric interval between

FIG. 7. (a) Braiding pattern in steady flow, $Re \sim 100$, as visualized by activating pH-sensitive dye at leading wire electrode, imbedded in the top wavy wall near the left edge of photograph. Field of view is located twelve geometric waves downstream from inlet. (b) At somewhat higher $Re \sim 250$, the same field shows a much more widely-spaced pattern of secondary Goertler vortices. (c) Periodic splitting and coalescence of this secondary pattern occurs 2 channel wavelengths downstream from dye origin for $250 < Re < 450$. All figures approx. same scale.

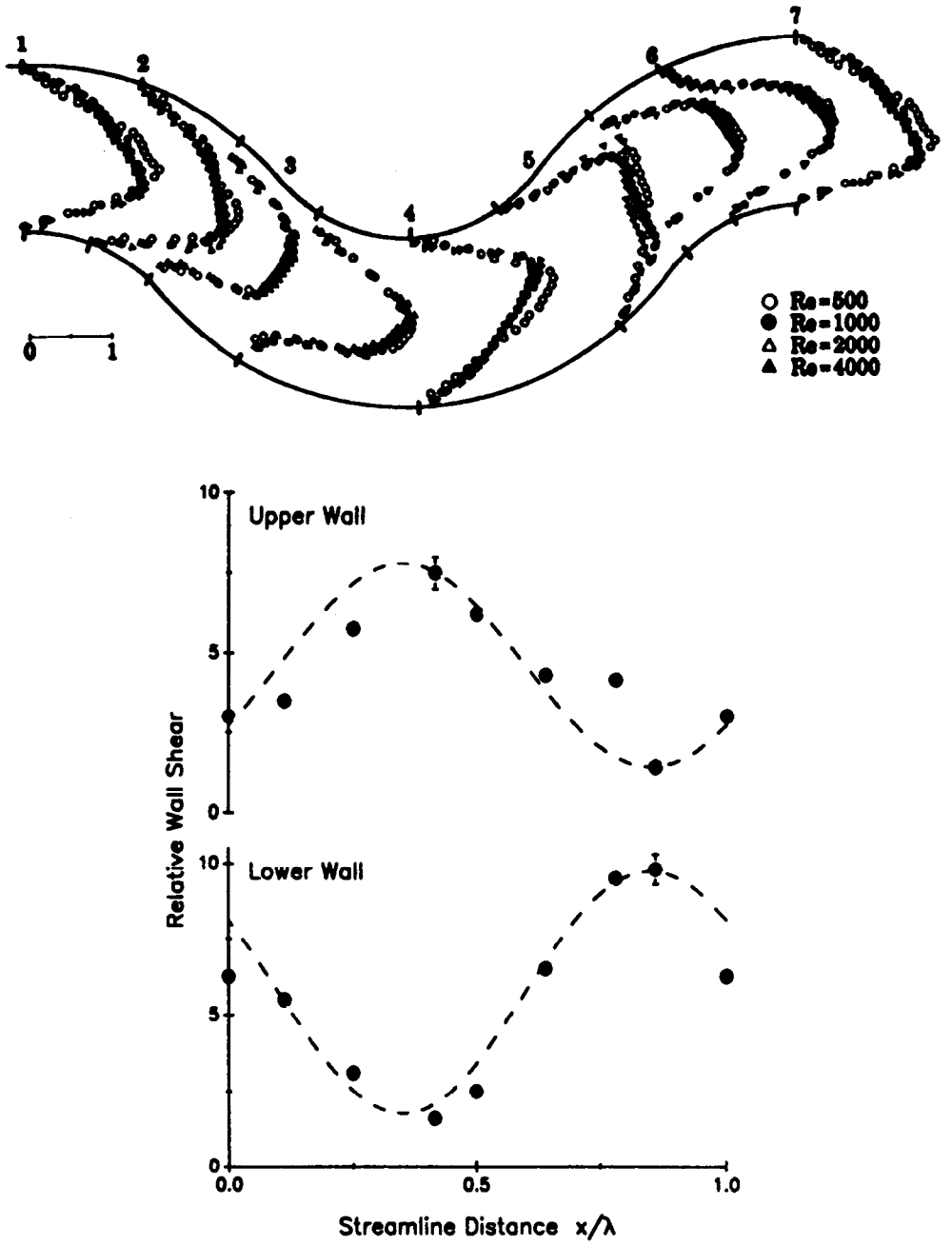

FIG. 8. Top panel: Sequence of axial velocity profiles in the fully-developed region of the test section, 12–14 wavelengths downstream from the entrance, by hot-wire anemometry. The streamwise dimension of channel walls is foreshortened for clarity. Numbered points on boundary correspond to locations of heat-flux gauges. Normalized velocity scale at left. Bottom panels: Sinusoidal variation of wall shear produced by these profiles. Dashed line for upper wall represents the expression $du/dy = 4.6+3.2\sin[2\pi(x/\lambda-0.1)]$; corresponding line for lower wall is $du/dy = 1.25\{4.6+3.2\sin[2\pi(x/\lambda+0.4)]\}$. Thus regions of high wall shear correspond to low heat flux in Fig. 9.

consecutive inflection points. Its main features seem to be governed by inviscid mechanisms, so that the phase difference between flow and geometry shifts less than 20° over an eightfold range in Reynolds number.

Viewed from the sidewalls, the flow pattern appeared to be disturbed and unsteady even at $Re = 1000$, although separated regions were not observed. We surmise that regions of back-flow must be quite localized, even though the wall spacing in the acrylic channel was found to vary widely

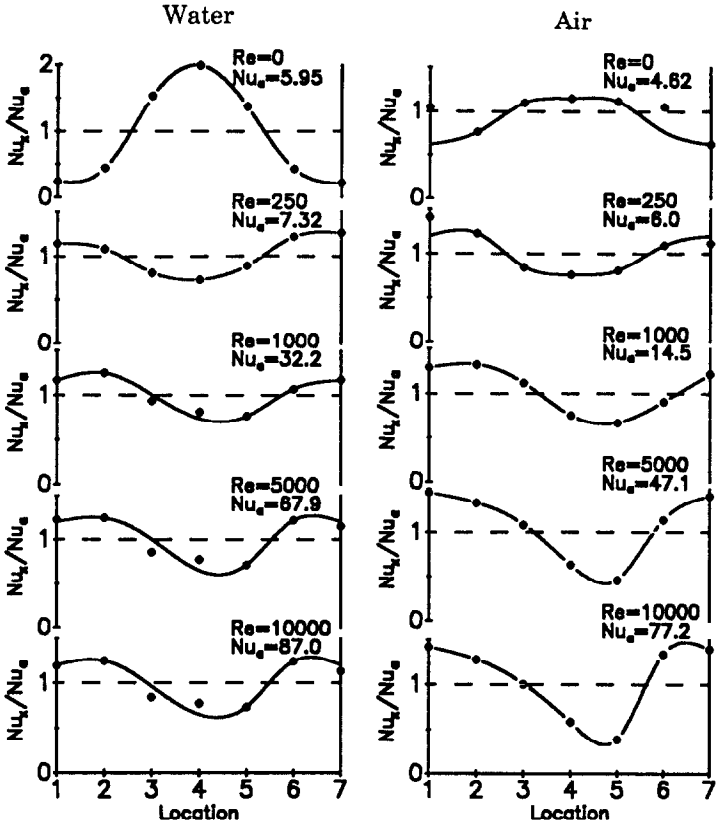

FIG. 9. Spatial variation of local Nu along the instrumented portion of channel for water (left panels) and air (right panels) at various Re, compared with segment average Nu_a. Peak values correspond to points 6–2 in Fig. 8 where wall shear is minimal.

($9.5 \leqslant H \leqslant 12$ mm).† The absence of significant flow separation in the face of a 15% variation in flow cross-section suggests that the serpentine design would be relatively resistant to performance degradation produced by misalignments of the channel walls during manufacture. A computational study of two-dimensional wavy-wall patterns indicates the onset of only slight separation at $Re \geqslant 500$ [10]. In contrast, both flow visualization [3] and simulation studies [11] show separation to be prevalent on a corrugated wall.

The above observations were useful in interpreting the measured patterns of local heat flux shown in Fig. 9. In the absence of flow ($Re = 0$) natural convection made the heat flux strongly non-uniform even though the heated surface was always kept topmost. Water typically exhibited a stronger, more symmetric effect due to higher Grashof number. Corresponding convection cells were observed to occupy the entire channel lumen and had a spanwise spacing approximately equal to the wall separation (10.5 mm). All cases for non-zero Re had $Gr/Re^2 < 1$, indicating that natural convection was of rapidly diminishing importance. This was confirmed by the abrupt change in distribution at non-zero Re. Like the velocity profiles, the thermal profiles became fully-developed only in a periodic sense: the spatial distributions of heat flux seen in Fig. 9 are highly non-uniform along the length of the instrumented segment despite the uniform surface temperatures. In comparing the two fluids a Pr effect of secondary flow seems to emerge at higher Re, but the peak flux always occurs in the region between points 6 and 2, where shear on the upper wall is nearly minimal. Likewise, local heat transfer is least between 4 and 5, where wall shear is greatest.

This impression was confirmed by evaluating the slope of each velocity profile near the wall to estimate the local shear. This procedure is necessarily somewhat qualitative since it is difficult to pinpoint the exact wall location, but the result summarized in the bottom panels of Fig. 8 seems clear-cut: in this channel geometry peak shear stress occurs approx. 145° out of phase with peak local heat flux.‡ Note that shear along the top and bottom walls is almost exactly 180° out of phase, consistent with the flow being periodically fully-developed. Applying mass conservation between successive axial profiles supplies one plaus-

†In the instrumented segment of the aluminum test section, the measured separation distance was 10.5 ± 0.2 mm.

‡The systematically greater values of shear obtained for the lower wall are probably due to local blockage, produced when the anemometer was fully inserted into the stream.

ible resolution: the growing shear in segment 6–3 implies that crossflow must be directed towards the wall. The impingement of relatively cooler bulk fluid increases local ΔT, giving rise to greater local heat transfer across the boundary layer. At peak values of shear this crossflow must vanish and heat flux thereby diminishes. The converse process occurs in segment 3–6, where heat transfer would be favored on the bottom wall. By this model, the phase difference between geometry and heat flux (in Fig. 9) suggests an asymmetry due to inertial lag, rather than to local flow separation.

The overall correspondence between Figs. 8 and 9 leaves little doubt that the periodic secondary flow is primarily responsible for the high heat fluxes obtained with the serpentine design. We propose that the recurrent geometry keeps the boundary layers thin while simultaneously inducing impingement currents. Minimal heat transfer occurs where impingement currents are adverse; but is still augmented because axial shear is maximal. While downstream Goertler vortices may contribute some upwelling and mixing at very low Re, they are obliterated at Re significantly below the onset of significant augmentation. McCormack *et al.* [12] have shown theoretically that perturbed axial velocities induced in the (unconfined) boundary layer of a singly curved bend should be two orders of magnitude greater than the transverse velocity components associated with Goertler vortices. Probably they only weakly augment heat transfer in a tightly-curved serpentine channel, although it would be useful to evaluate their effect computationally, utilizing a two-dimensional simulation in which their action could be artificially suppressed.

HEAT TRANSFER—PRESSURE DROP

The Re-dependence of wall Nusselt numbers and channel friction factors in the fully-developed region is compared with that of a flat-wall channel in Figs. 10(a) and (b). The indicated error brackets are typical. Discounting natural convection, both Nu and f appear to converge to flat-wall behavior at low Re but become significantly greater for $Re > 500$. At Re somewhat beyond the experimental range Nu probably becomes comparable to values predicted by the Dittus–Boelter correlation for channel flow, and therefore may be attributable to turbulent motions. In the laminar-transitional regime, however, augmentation is surely due to the relatively greater importance of the secondary flows. Peak enhancement occurs at $Re = 3200$, where heat transfer in the wavy-wall channel is 9.4 and 14.2 times greater than in a laminar-flow flat-wall design, for air and water respectively. Corresponding pressure drops are about five times greater.

Owing to the complex flow structure, the Pr-dependence of our heat-transfer coefficients varies distinctly from standard form. The following expression was found adequate to within experimental accuracy for $Re > 250$:

$$Nu = 4 + 29.2 \ln [(Re\, Pr^{0.4} + 1000)/1200]. \quad (1)$$

This form was chosen to represent the effect of secondary flows separately from the effect of conduction, which is given by the first term on the RHS of the equation. The Pr-dependence in the second term is similar to better-known correlations although the added offset is necessary to reproduce the relatively abrupt increase in augmentation at $Re \sim 1000$. Other than for design purposes we attach no special significance to this correlation, although it is interesting that our data show no distinction between laminar and transitional flow behavior. We shall see that it also succeeds in correlating the data obtained by Kays and London [13] for a similar channel design.

An operational measure of performance is obtained by comparing Nusselt numbers on an equal pumping-power basis, $f Re^3$ [14], as is done in Fig. 10(c). Compared to a flat-wall channel, the serpentine section yields significantly improved performance at all Reynolds numbers greater than 500. In particular, at $f Re^3 = 2.45 \times 10^8$ ($Re = 2000$) the net enhancement can be expected to reach 600% for air and 1040% for water. This benefit requires no increase in size and only a 7.8% increase in exchanger plate material. For applications in which heat transfer is paramount and flow rate incidental, Nu may be a specified design parameter and pumping power considered as a cost. The serpentine channel typically provides a 40-fold reduction in pumping power, as can be seen by holding Nu fixed in Fig. 10(c).

DISCUSSION

Our experiments utilized measurements of heat flux in the thermally fully-developed region of a single uniformly heated surface, and therefore cannot be directly applied to assess the heat transfer rate in a parallel-wall channel. It would be desirable, however, to compare our results with published studies of symmetrically-heated walls, so as to predict at least approximately how well the wavy-wall design might perform as a heat-exchanger. To do so we need to relate Nu obtained from asymmetric boundary conditions to values for symmetric boundary conditions. As an example, we note that a single heated wall in laminar flow, at constant temperature, yields $Nu = 4$. Two such walls placed in parallel to form a channel would be expected to yield $Nu = 8$, since the heat flux to the fluid has now doubled. This estimate is within 6% of the exact value, $Nu = 7.55$, for a symmetrically-heated channel and suggests the use of a factor $7.55/4 = 1.9$. Owing to effects of Pr number, symmetrically-heated channels are less efficient than this in transitional and turbulent regimes. Computational results for flat-wall heat exchangers at $Re = 7000$ yield symmetric Nu approximately 1.3–1.5 times the asymmetric Nu for water and air respectively [15]. Thus we

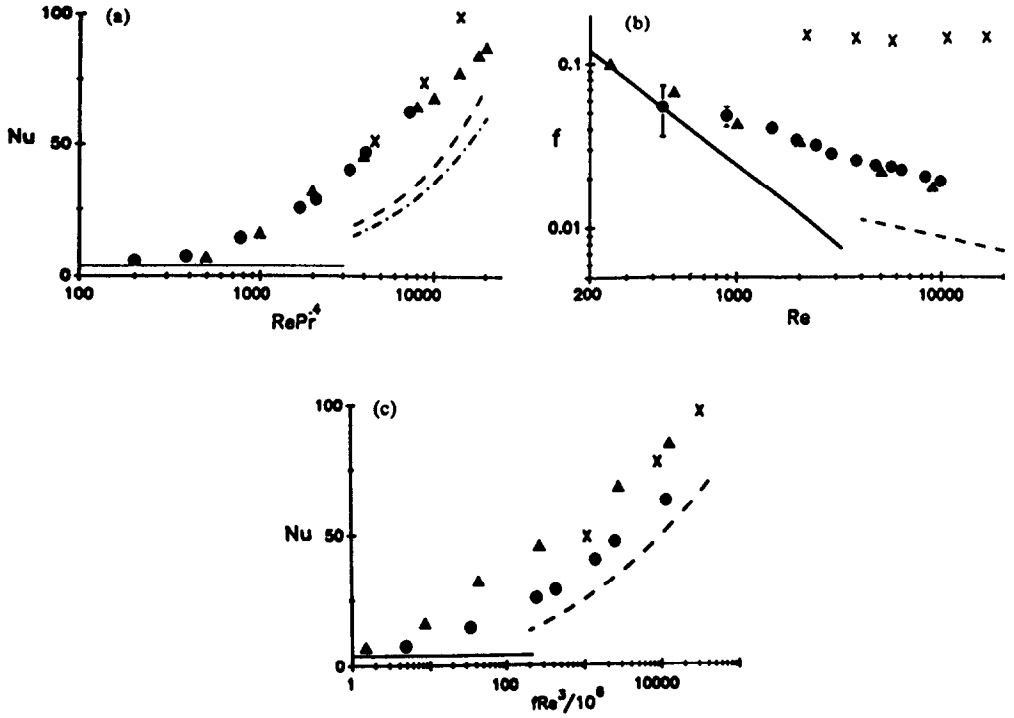

FIG. 10. (a) *Re*-dependence of *Nu* and (b) Fanning friction factor for serpentine channel. Circles: air; triangles: water. Laminar regime for a flat-wall channel is depicted by solid line; turbulent Dittus–Boelter correlations for water and air are given by dashed lines. Crosses: data for a sharply-corrugated channel [3], with *Nu* divided by 1.5 to compare with singly-heated wall. (c) Equal-pumping-power comparison of heat transfer performance for serpentine channel with a flat-wall channel and sharply-corrugated channel. Peak augmentation is 600% for air and 1040% for water at $Re = 2000$. An equal heat-load comparison can be performed by holding *Nu* constant. At $Nu = 25$, pumping power is reduced 40-fold.

expect that in the transitional regime our experimental results can be related at least approximately to similar compact heat exchangers by dividing published values of *Nu* by 1.5.

Kays and London have measured friction factors and pressure drops, in air, for many compact heat exchanger designs, including a moderately-corrugated wall geometry (surface designation 17.8–3/8 W) with channel spacing $H = 1.43$ mm. Its periodicity $\lambda/H = 6.67$, peak-to-peak amplitude $b/H = 2.28$, and centerline curvature ratio $R/(H/2) \sim 4.7$ are all similar to the serpentine channel parameters. Dividing their data by the factor 1.5 permits a direct comparison utilizing the correlation given by equation (1), resulting in a slope of 10.1 rather than 29.2. Heat transfer in our test section increases faster with *Re* and therefore yields a somewhat superior performance in the laminar-transitional flow regime. This difference is underestimated since only an overall *Nu* is reported for channel 17.8–3/8W. Kays and London attributed the effectiveness of their design to the induction of flow separation on the leeward edges of the wave crests. Even at high *Re*, however, their measured friction factors are only 10% greater than for serpentine design; and therefore are probably smaller than would be obtained if flow separation had been complete (see below).

A clearer case for flow separation as a dominant heat-transfer mechanism is made by the corrugated-wall channel of O'Brien and Sparrow, which also has a global geometry similar to ours but with sharply acute corners rather than analogous wave crests and troughs. These authors inferred from visualized stream patterns that flow separation was sufficiently prominent to render the flow essentially two-dimensional; although Goldstein and Sparrow [7] found some spanwise variation in mass-transfer rates associated with Goertler arrays. As shown in Fig. 10(b), friction factors were much higher than in the serpentine channel: typically, by threefold at $Re = 2000$ and sevenfold at $Re = 10\,000$. Corresponding *Nu*, however, were also greater; so that the corrugated channel design yields an equivalent or better overall performance when viewed on an equal-pumping-power basis in Fig. 10(c). Sparrow and Hossfield [16] reported that heat transfer was much diminished after rounding off the sharp-edged corners, thereby demonstrating that full separation produces an optimal operating point. This finding still leaves open, however, the possibility that suppression of flow separation might lead to a different optimal operating point.

Is there a low-*Re*-number regime within which secondary flow in the serpentine channel outperforms

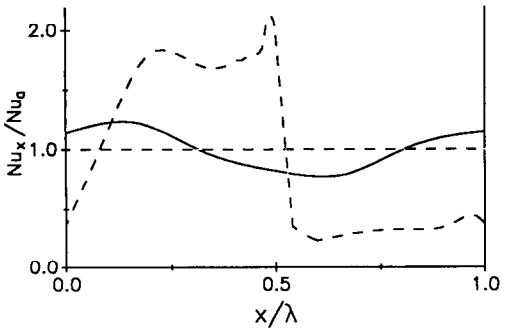

FIG. 11. Comparison of heat-flux distribution obtained experimentally using water (solid line; $Nu_a = 16.4$), with two-dimensional computations [11] for corrugated wall geometry (dashed line; $Nu_a = 10.2/1.5 = 6.8$) witih periodicity $\lambda/H \sim 4$. $Re \sim 500$ for both cases.

flow separation? Ramadhyani [11] carried out two-dimensional low-*Re* simulations on corrugated ducts similar to those of Sparrow and his co-workers. His results substantiate the experimental findings of Goldstein and Sparrow that flow separation, all by itself, can provide only a modest augmentation of heat transfer at low *Re*. A typical case is shown in Fig. 11 for $(H/L) = 0.23$ and $\theta = 22°$, corresponding approximately to an equivalent serpentine periodicity $\lambda/H \sim 4$. Flow separation is clearly evident on the leeward side of the wave crests, producing a heat flux distribution which looks much more non-uniform than our measured distribution at comparable *Re* and *Pr*. In the absence of flow separation the friction factor for the serpentine channel is half as large, and the average *Nu* about twice as great. Impingement currents induce high heat transfer on the upstream segment of the wavy-wall surface; peak shear stress increases heat flux on the leeward segment. The contrast with the computational study suggests why overall enhancement in the serpentine channel is improved relative to the moderately-corrugated design of Kays and London, in the laminar-transitional regime.

It seems clear from these separate investigations that different flow mechanisms may play starring roles in promoting heat transfer, depending crucially on operating regime and local details of surface geometry. Flow patterns in corrugated and wavy-wall ducts may become so complex that identifying their importance to augmentation can only be inferred indirectly, through a comparison with simplified computational studies of two-dimensional viscous flow in which swirling patterns are incapable of forming.

CONCLUSIONS

Several competing mechanisms are held to enhance heat transfer in spoiled-geometry parallel-wall ducts. The simulation models of Ramadhyani and Garg and Maji illustrate that two-dimensional flows produce significant enhancement at low *Re* in a corrugated or wavy-wall channel similar to our own. In the experiments of Sparrow and co-workers flow separation in such channels occurs on the leeward side of wave crests, but this is more than compensated for by the upstream impingement of strong currents. Entrained corner vortices may also provide significant enhancement in commercial applications as utilized by Kays and London. In complex geometries, therefore, a variety of mechanisms have the potential to form useful secondary flows. The design described in this report is novel in that boundary-layer growth is repetitively interrupted by the wall curvature to promote augmented heat transfer; while flow separation is suppressed to minimize loss.

Acknowledgements—The authors wish to thank Dr Phil Ligrani of the University of Utah for help on several points. This research was sponsored by the Physical Sciences and Industrial Utilization Departments of the Gas Research Institute, whose support is gratefully acknowledged.

REFERENCES

1. Y. Mori and W. Nakayama, Recent advances in compact heat exchangers in Japan. In *Compact Heat Exchangers—History, Technological Advancement and Mechanical Design Problems* (Edited by R. K. Shah *et al.*), *ASME HTD*-Vol. 10, pp. 5–16 (1980).
2. H. M. Joshi and R. L. Webb, Heat transfer and friction in the offset strip-fin heat exchanger, *Int. J. Heat Mass Transfer* **30,** 69–84 (1987).
3. J. E. O'Brien and E. M. Sparrow, Corrugated-duct heat transfer, pressure drop, and flow visualization, *ASME J. Heat Transfer* **104,** 410–416 (1982).
4. I. J. Sobey, On flow through furrowed channels. Part 1. Calculated flow patterns, *J. Fluid Mech.* **96,** 1–26 (1980).
5. M. Greiner, R. F. Chen and R. A. Wirtz, Heat transfer augmentation through wall shape induced flow destabilization. In *Heat Transfer in Convective Flows* (Edited by R. K. Shah), *ASME HTD*-Vol. 107, pp. 336–341 (1990).
6. G. E. Karniadakis, B. B. Mikic and A. T. Patera, Minimum-dissipation transport enhancement by flow destabilization: Reynolds' analogy revisited, *J. Fluid Mech.* **192,** 365–391 (1988).
7. L. Goldstein and E. M. Sparrow, Heat/mass transfer characteristics for flow in a corrugated wall channel, *ASME J. Heat Transfer* **99,** 187–195 (1977).
8. W. S. Saric, V. Kalbirgi and J. R. Dagenhart, Goertler instability with periodic curvature, *Bulletin of the American Physical Society, Series II* **33,** 2283 (1988).
9. J. D. Swearington and R. Blackwelder, The growth and breakdown of streamwise vortices in the presence of a wall, *J. Fluid Mech.* **182,** 255–290 (1987).
10. V. K. Garg and P. K. Maji, Flow and heat transfer in a sinusoidally curved channel, *Int. J. Engng Fluid Mech.* **1,** 293–319 (1988).
11. S. Ramadhyani, Numerical prediction of flow and heat transfer in corrugated ducts. In *Advances in Heat Exchanger Design* (Edited by R. K. Shah and J. T. Pearson), *ASME HTD*-Vol. 66, pp. 37–43 (1987).
12. P. D. McCormack, H. Welker and M. Kelleher, Taylor–Goertler vortices and their effect on heat transfer, *ASME J. Heat Transfer* **92,** 101–112 (1970).
13. W. M. Kays and A. L. London, *Compact Heat Exchangers* (3rd Edn), p. 204. McGraw-Hill, New York (1984).

14. J. G. Soland, W. M. Mack, Jr. and W. M. Rohsenow, Performance ranking of plate-fin heat exchanger surfaces, *ASME J. Heat Transfer* **100**, 514–519 (1978).
15. A. P. Hatton and A. Quarmby, The effect of axially varying and unsymmetrical boundary conditions on heat transfer with turbulent flow between parallel plates, *Int. J. Heat Mass Transfer* **6**, 903–914 (1963).
16. E. M. Sparrow and L. M. Hossfield, Effect of rounding of protruding edges on heat transfer and pressure drop in a duct, *Int. J. Heat Mass Transfer* **27**, 1715–1723 (1984).